

Comparative Study of Robust RSC Control of Doubly Fed Induction Generator Based Wind Turbine under Grid Frequency and Voltage Variations

Hakima Bahlouli^{1*}, Abdellah Mansouri², Mohamed Bouhamida¹

¹ Laboratoire d'Automatisation Vision et Contrôle des Systèmes AVCIS, Automation Département, Université des Sciences et de la Technologie d'Oran Mohamed-Boudiaf, El Mnaouar, 31000 Bir El Djir, P.O.B. 1505, Oran, Algeria

² Laboratoire d'Automatique et d'Analyse des Systèmes LAAS, Département de Génie Électrique, École Nationale Polytechnique d'Oran Maurice Audin, El Mnaouar, 31000 Bir El Djir, P.O.B. 1523, Oran, Algeria

* Corresponding author, e-mail: hakima.bahlouli@univ-usto.dz

Received: 12 October 2022, Accepted: 15 May 2023, Published online: 17 July 2023

Abstract

The configuration of a grid-connected doubly fed induction generator (DFIG) for wind energy generation systems consists of direct coupling of the generator stator windings with the grid and partial coupling of the rotor through power converters. This structure makes the system sensitive to the fault grid. Thus, robust control techniques are required to deal with the undesirable transient sequences in the network. In this paper, two robust controllers have integrated to regulate the stator active and reactive power of DFIG based wind turbine. Then, they have been tested and compared to verify their performances when abnormal grid networks have occurred. Firstly, we used high order sliding mode (HOSM) based Super Twisting, which keeps the same conventional sliding mode performances, such as fast dynamic response and redundancy to the external disturbances, with a simple design and chattering reduction. Secondly, we implement the backstepping control approach which is known for its robustness in transient sequences. A number of simulations have carried out to evaluate the ride-through performance of both control strategies in case of low grid voltage dips and grid frequency variations.

Keywords

high order sliding mode, backstepping, DFIG, fault ride-through capability, super twisting algorithm

1 Introduction

The wind power plants must operate as conventional plants. Thence the electrical grid requirements applied for the existing power plants are also used for wind farms.

Grid code is a technical specification that defines requirements for power producers to be allowed to connect to an electrical network and has to satisfy and ensure the safety, security and economic functioning of the power system. Contents of this code depend on the transmission company requirement [1, 2].

The most common technical requirements for wind power generators are [3]:

- fault ride-through requirements,
- active and reactive power responses following disturbances,
- extended variation range for the voltage-frequency,
- active power control or frequency regulation support,
- reactive power control or voltage regulation capability.

Currently, most of wind energy generation systems (WEGs), producing more than 1MW, are based on a doubly fed induction generator (DFIG). The stator of such a generator is directly connected to the utility grid. The electrical rotor, equipped with windings, is connected through a set of slip rings to two back-to-back converters (rotor side converter and grid side converter) sharing the DC bus. This configuration is attractive as it allows for the power electronic converter to deal with around 30% of the generated power instead of the total power generated (Fig. 1) [4–6]. Being connected directly to the grid through a stator makes the generator very sensitive to the grid faults.

The sliding mode control technique is suitable to regulate the DFIG based wind turbine (DFIG-WT) due to its features of finite-time convergence and robustness against disturbances [7]. This robust control achieves satisfactory results. However, it is affected by the chattering

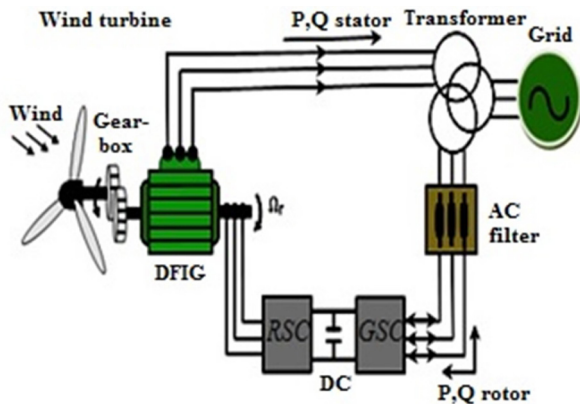


Fig. 1 System configuration of the DFIM based wind turbine

phenomenon caused by the switching term. Many works have been conducted to improve the control algorithm to reduce this phenomenon [8–10]. Furthermore, the high order sliding mode (HOSM) control algorithm has been a good alternative to the conventional sliding mode with chattering free [11, 12]. HOSM based on super twisting is one of the popular and robust controllers with simple algorithm implementation; the idea of this technique is to let the discontinuous control act on the higher-order derivatives of the sliding variable [13–16].

Other recommended control method is backstepping, it is a recursive method of minimizing control effort, which combines a Lyapunov function with the structure of a feedback loop. The method consists in transforming intermediate state variables into virtual inputs that will control other state variables and reduce the order of complex systems into several lower-order simple systems which assure very good dynamic during a transient regime [17, 18].

In this context, the purpose of this work is to test two robust control methods under abnormal conditions of the network with no additional hardware. Firstly, the paper presents a dynamic model of DFIG used in wind generator systems, the mathematical model is developed using a field-oriented control technique this technique allows to transform the three components into two orthogonal components which can be considered as vectors [19].

Thereafter, two control techniques is developed to control the stator active and reactive powers through rotor side converter, first technique used is backstepping, and the second one is HOSM based on the super twisting algorithm. These two controllers are common robust methods used to control DFIG-WT.

At last, a test of the performances is undertaken for both controllers under low voltage dips and frequency variation.

2 DFIG dynamic modeling in the d - q reference frame

The generator's dynamic model is defined in the synchronous d - q frame using Park's transformation as detailed in [20].

The expressions of stator and rotor voltages are given as follows (Eqs. (1)–(4)):

$$v_{sd} = R_s i_{sd} + d\varphi_{sd} / dt - w_s \varphi_{sq}, \quad (1)$$

$$v_{sq} = R_s i_{sq} + d\varphi_{sq} / dt + w_s \varphi_{sd}, \quad (2)$$

$$v_{rd} = R_r i_{rd} + d\varphi_{rd} / dt - w_r \varphi_{rq}, \quad (3)$$

$$v_{rq} = R_r i_{rq} + d\varphi_{rq} / dt + w_r \varphi_{rd}. \quad (4)$$

where: $w_r = g w_s$.

The stator and rotor fluxes are defined as (Eqs. (5)–(8)):

$$\varphi_{sd} = L_s i_{sd} + L_m i_{rd}, \quad (5)$$

$$\varphi_{sq} = L_s i_{sq} + L_m i_{rq}, \quad (6)$$

$$\varphi_{rd} = L_r i_{rd} + L_m i_{sd}, \quad (7)$$

$$\varphi_{rq} = L_r i_{rq} + L_m i_{sq}. \quad (8)$$

The stator and rotor active and reactive power are expressed as (Eqs. (9)–(12)):

$$P_s = v_{sd} i_{sd} + v_{sq} i_{sq}, \quad (9)$$

$$Q_s = v_{sq} i_{sd} - v_{sd} i_{sq}, \quad (10)$$

$$P_r = v_{rd} i_{rd} + v_{rq} i_{rq}, \quad (11)$$

$$Q_r = v_{rq} i_{rd} - v_{rd} i_{rq}. \quad (12)$$

3 Controllers design

In order to control the active and reactive power of the stator, we have to decouple them first. For that we proceed to control the current space vector directly in the d - q reference frame of the rotor by mean of field-oriented technique [21, 22]. The technique's main principle is to orientate the stator flux on d axis as illustrated in Fig. 2.

Thus, the stator flux and voltage are expressed as follow:

$$\varphi_{sd} = \varphi_s; \quad \varphi_{sq} = 0; \quad v_{sq} = v_s = \varphi_s w_s; \quad v_{sd} = 0.$$

Then the Eqs. (5) and (6) become:

$$\varphi_s = L_s i_{sd} + L_m i_{rd}, \quad (13)$$

$$0 = L_s i_{sq} + L_m i_{rq}. \quad (14)$$

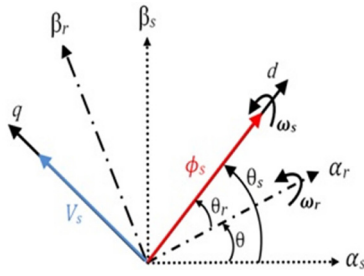


Fig. 2 Orientation of the stator flux on the axis d

We write the expressions relating stator currents to rotor currents as follows (Eqs. (15) and (16)):

$$i_{sq} = -L_m / L_s i_{rq}, \quad (15)$$

$$i_{sd} = v_s / (w_s L_s) - L_m / L_s i_{rd}. \quad (16)$$

Substituting stator currents in Eqs. (7) and (8) by their expressions (Eqs. (15) and (16)), we obtain:

$$\varphi_{rd} = L_m v_s / (w_s L_s) + L_r \sigma i_{rd}, \quad (17)$$

$$\varphi_{rq} = L_r \sigma i_{rq}. \quad (18)$$

We introduce these last Eqs. (17) and (18) in rotor voltages expressions (Eqs. (3) and (4)):

$$v_{rd} = R_r i_{rd} + L_r \sigma di_{rd} / dt - w_r L_r \sigma i_{rq}, \quad (19)$$

$$v_{rq} = R_r i_{rq} + L_r \sigma di_{rq} / dt + w_r L_r \sigma i_{rd} + w_r L_m v_s / (w_s L_s). \quad (20)$$

Or:

$$di_{rd} / dt = (v_{rd} - R_r i_{rd} + w_r L_r \sigma i_{rq}) / L_r \sigma, \quad (21)$$

$$di_{rq} / dt = \begin{pmatrix} v_{rq} - R_r i_{rq} - w_r L_r \sigma i_{rd} \\ -w_r L_m v_s / (w_s L_s) \end{pmatrix} / L_r \sigma. \quad (22)$$

Then, the adaptation of the Eqs. (9) and (10) of the active and reactive powers to the technique method and to the simplifying assumptions made in our case, gives:

$$P_s = -v_s L_m / L_s i_{rq}, \quad (23)$$

$$Q_s = v_s^2 / (L_s w_s) - v_s L_m / L_s i_{rd}. \quad (24)$$

3.1 Backstepping controller design

In Section 3.1, backstepping controller based on vector control technique will be developed.

The tracking errors are defined by:

$$\begin{cases} e_{ps} = P_s^{ref} - P_s \\ e_{qs} = Q_s^{ref} - Q_s \end{cases} \quad (25)$$

Let us consider the following Lyapunov function:

$$\begin{cases} V(e_{ps}) = \frac{1}{2} e_{ps}^2 \\ V(e_{qs}) = \frac{1}{2} e_{qs}^2 \end{cases} \quad (26)$$

The derivative of Lyapunov's function:

$$\begin{cases} \dot{V}(e_{ps}) = e_{ps} \dot{e}_{ps} \\ \dot{V}(e_{qs}) = e_{qs} \dot{e}_{qs} \end{cases} \quad (27)$$

$$\begin{cases} \dot{V}(e_{ps}) = e_{ps} \left(\dot{P}_s^{ref} + v_s \frac{L_m}{L_s} \frac{di_{rq}}{dt} \right) \\ \dot{V}(e_{qs}) = e_{qs} \left(\dot{Q}_s^{ref} + v_s \frac{L_m}{L_s} \frac{di_{rd}}{dt} \right) \end{cases} \quad (28)$$

Then we get the stabilizing control laws as follows:

$$\begin{cases} v_{rq} = \frac{-L_s L_r \sigma}{v_s L_m} (\dot{P}_s^{ref} + K_1 e_{ps}) \\ + R_r i_{rq} + w_r L_r \sigma i_{rd} + \frac{w_r L_m v_s}{w_s L_s} \\ v_{rd} = \frac{-L_s L_r \sigma}{v_s L_m} (\dot{Q}_s^{ref} + K_2 e_{qs}) \\ + R_r i_{rd} - w_r L_r \sigma i_{rq} \end{cases} \quad (29)$$

To ensure the convergence of Lyapunov's function, we replace Eq. (29) in the derivative of Lyapunov's function Eq. (28) respectively, we obtain:

$$\begin{cases} \dot{V}(e_{ps}) = -K_1 e_{ps}^2 < 0 \\ \dot{V}(e_{qs}) = -K_2 e_{qs}^2 < 0 \end{cases} \quad (30)$$

where K_1 and K_2 are constant positive values.

3.2 High order sliding mode control design for active and reactive power

In order to optimize the active and reactive power, the sliding surfaces are given by:

$$\begin{cases} e_{ps} = P_s^{ref} - P_s \\ e_{qs} = Q_s^{ref} - Q_s \end{cases} \quad (31)$$

Then we will have:

$$\begin{cases} \dot{e}_{ps} = \dot{P}_s^{ref} + v_s \frac{L_m}{L_s} \frac{di_{rq}}{dt} \\ \dot{e}_{qs} = \dot{Q}_s^{ref} + v_s \frac{L_m}{L_s} \frac{di_{rd}}{dt} \end{cases} \quad (32)$$

and:

$$\begin{cases} \dot{e}_{ps} = \dot{P}_s^{ref} + \frac{v_s L_m}{L_s L_r \sigma} \begin{pmatrix} v_{rq} - R_r i_{rq} \\ -w_r L_r \sigma i_{rd} \\ -\frac{w_r L_m v_s}{L_s L_s} \end{pmatrix} \\ \dot{e}_{qs} = \dot{Q}_s^{ref} + \frac{v_s L_m}{L_s L_r \sigma} \begin{pmatrix} v_{rd} - R_r i_{rd} \\ -w_r L_r \sigma i_{rq} \end{pmatrix} \end{cases} \quad (33)$$

If we define the functions F and G as follow:

$$\begin{cases} F_1 = \frac{v_s L_m}{L_r \sigma L_s} \\ G_1 = \dot{P}_s^{ref} + \frac{v_s L_m}{L_r \sigma L_s} \begin{pmatrix} -R_r i_{rd} - w_r L_r \sigma i_{rd} \\ -\frac{w_r v_s L_m}{L_s w_s} \end{pmatrix} \end{cases} \quad (34)$$

$$\begin{cases} F_2 = \frac{v_s L_m}{L_r \sigma L_s} \\ G_2 = \dot{Q}_s^{ref} + \frac{v_s L_m}{L_r \sigma L_s} (-R_r i_{rd} + w_r L_r \sigma i_{rq}) \end{cases} \quad (35)$$

Thus, we have: $\ddot{e} = F \dot{u} + \dot{G}$.

Consequently, we consider the following high order sliding mode controller based on the super twisting algorithm:

$$\begin{cases} v_{rq} = y_1 - B_1 |e_{ps}|^{0.5} \text{sign}(e_{ps}) \\ \dot{y}_1 = -B_2 \text{sign}(e_{ps}) \\ v_{rd} = y_2 - B_3 |e_{qs}|^{0.5} \text{sign}(e_{qs}) \\ \dot{y}_2 = -B_4 \text{sign}(e_{qs}) \end{cases} \quad (36)$$

where the gains:

$$B_{2,4} > \frac{\phi_i}{\Gamma_{mi}} \quad i = 1, 2,$$

$$B_{1,3}^2 \geq \frac{4\phi_i \Gamma_{Mi} (B_{2,4} + \phi_i)}{\Gamma_{mi}^3 (B_{2,4} - \phi_i)},$$

$$|\dot{G}_i| < \phi_i,$$

$$0 < \Gamma_{mi} \leq F_i \leq \Gamma_{Mi}.$$

Γ_{mi} , Γ_{Mi} and ϕ_i are positive constants.

4 Simulation and results

Simulations to show the performances of two robust controllers under grid dips and frequency variation is carried out; the HOSM and backstepping regulators are respectively

implemented to control the active and reactive stator powers. Fig. 3 shows the schematic diagram of the studied system. The nominal parameters of the DFIG and wind turbine system are listed in Appendix.

The wind turbine blades are commonly designed to operate the DFIG near the synchronous speed. We consider the speed of wind is 8 m/s to have a realistic performance analysis.

Fault ride through is wind power generator capability to stay connected in voltage or frequency variations. To evaluate the performance of the previous controllers, we have considered several grid faults that might affect the presented power system.

The voltage dips usually occurred in the grid is divided into symmetrical and unsymmetrical faults. The symmetrical faults are extremely severe [23].

The faults simulated are:

1. A three-phase voltage dip of 50% during 0.2 s;
2. A two-phase voltage dip of 50% during 0.2 s (phase a and b);
3. A single-phase voltage dip of 50% during 0.2 s (phase a);
4. Frequency variation from 50 Hz to 47.5 Hz for 150 ms.

Case 1: Three-phase faults: Figs. 4–7 show the system response to a 50% grid voltage dip between 8 s and 8.2 s for the controllers (HOSM and backstepping control). Both controllers show good results of time recovering after the voltage dip. The overshoot of rotor speed with the HOSM controller is smaller compared to the backstepping controller. The same remark is observed for electromagnetic torque, stator active and reactive powers.

The range currents are acceptable for both controllers during the voltage dip even though we did not regulate

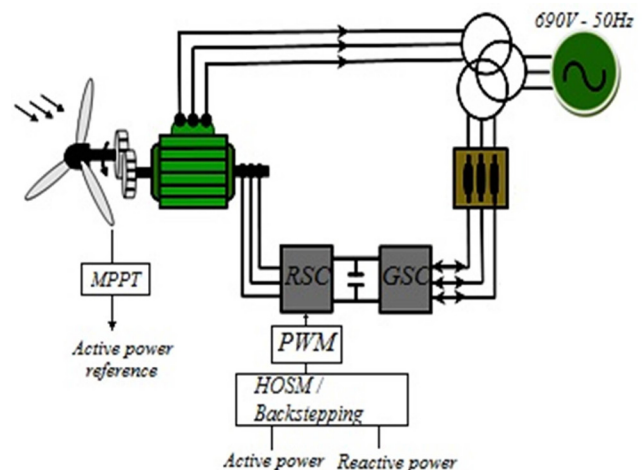


Fig. 3 Block diagram of RSC control of DFIG

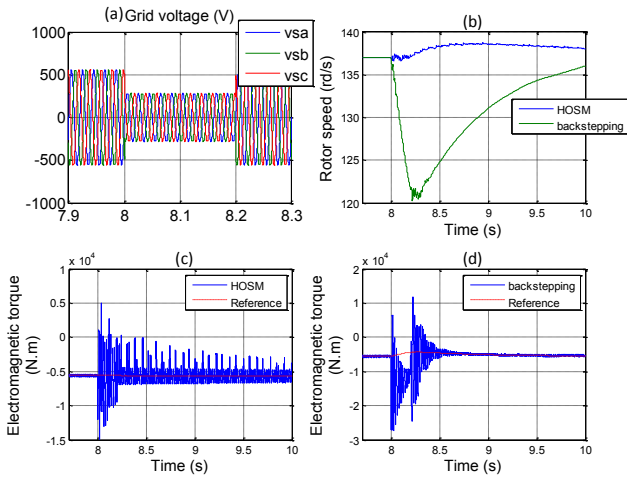


Fig. 4 Results of Case 1; (a) Three-phases voltage dips (50% faults) (V); (b) Rotor speed (rd/s), (c) Electromagnetic torque response of HOSM controller (N m); (d) Electromagnetic torque response of backstepping controller (N m)

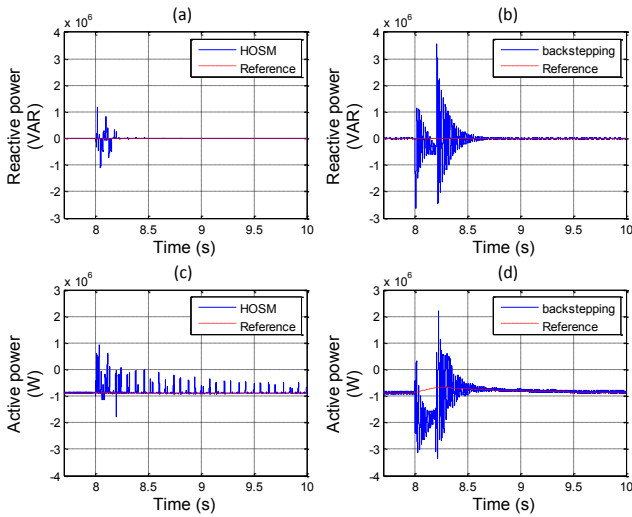


Fig. 5 Results of Case 1; (a) Reactive stator power response of HOSM controller (VAR); (b) Reactive stator power response of backstepping controller (VAR); (c) Active stator power response of HOSM controller (W); (d) Active stator power response of Backstepping controller (W)

the rotor currents as usually recommended. The HOSM controller recovers directly after the voltage dip. However, undesirable chattering appears.

Despite that the grid side converter is regulated by conventional PI in both systems, we notice that the DC-link voltage response of the system regulated by the HOSM technique is low sensitive to the transient regime than the other controlled system.

Case 2: Two-phase faults: Figs. 8–11 reveal the system response to 50% depth of grid voltage at phases "a" and "b" between 8 s and 8.2 s for both controllers. The HOSM still maintain a low overshoot than backstepping for rotor speed, electromagnetic torque, stator reactive and active

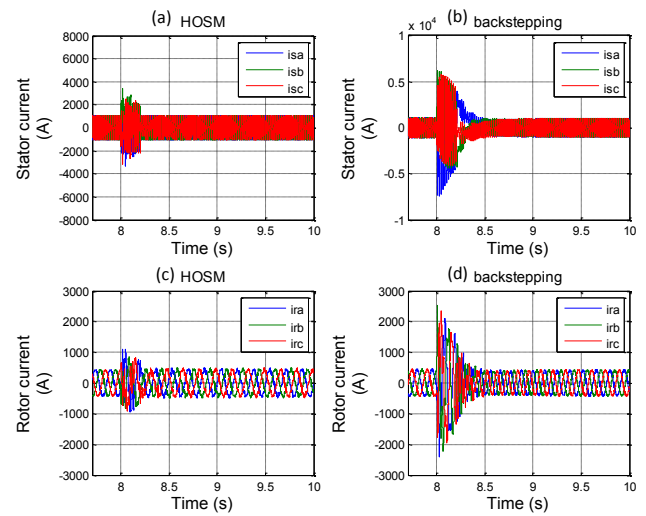


Fig. 6 Results of Case 1; (a) Stator current of HOSM controller (A); (b) Stator current of Backstepping controller; (c) Rotor current of HOSM controller (A); (d) Rotor current of Backstepping controller

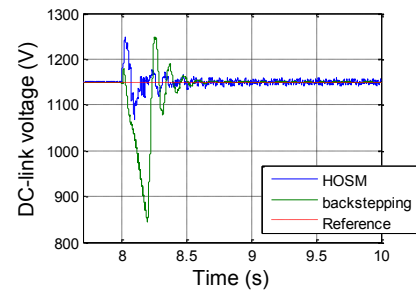


Fig. 7 DC-link voltage for HOSM and backstepping control (V) (Case 1)

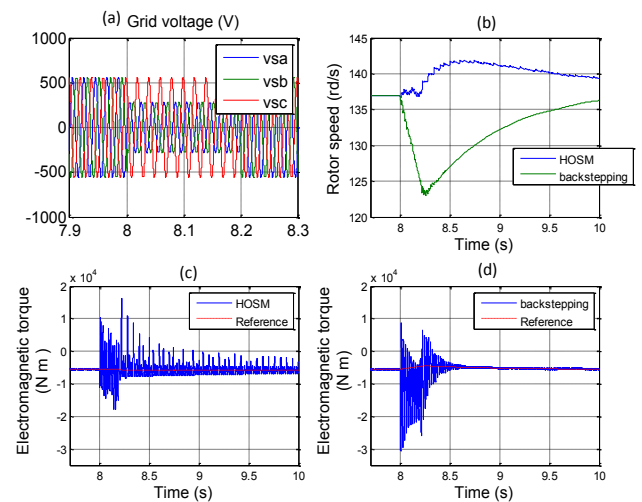


Fig. 8 Results of case 2; (a) Two-phases voltage dips (50% faults) (V); (b) Rotor speed (rd/s); (c) Electromagnetic torque of HOSM controller (N m); (d) Electromagnetic torque of Backstepping controller (N m)

power. Compared to the first case the HOSM is low effective in unbalanced voltage dip.

Upon evaluating the system's performance under both control techniques, it was found that the current responses

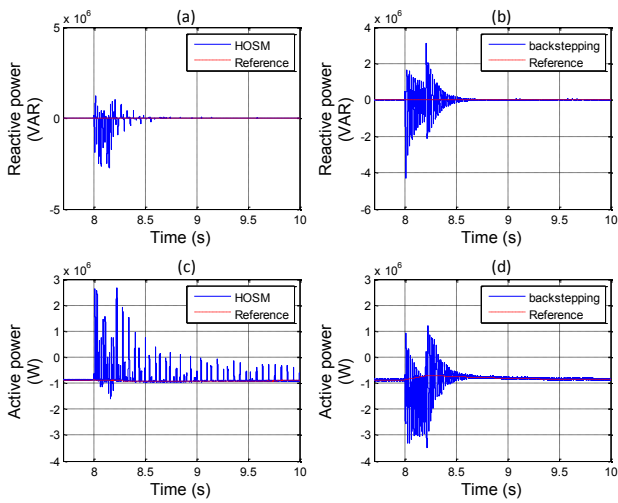


Fig. 9 Results of Case 2; (a) Reactive stator power response of HOSM controller (VAR); (b) Reactive stator power response of Backstepping controller (VAR); (c) Active stator power response of HOSM controller (W), (d) Active stator power response of backstepping controller (W)

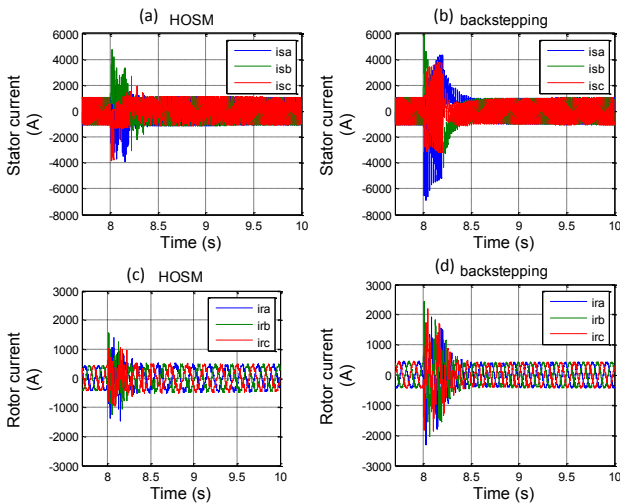


Fig. 10 Results of Case 2; (a) Stator current of HOSM controller (A); (b) Stator current of Backstepping controller; (c) Rotor current of HOSM controller (A); (d) Rotor current of Backstepping controller

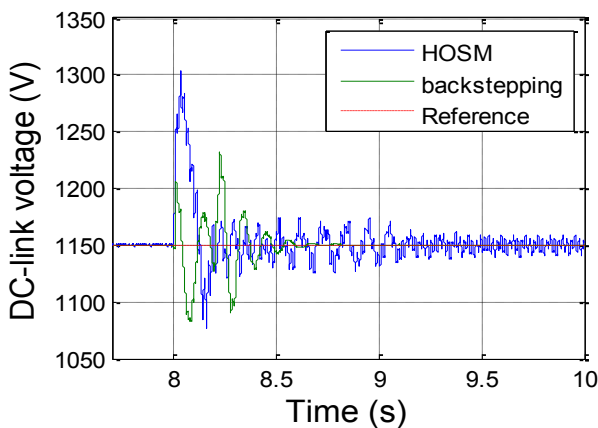


Fig. 11 DC-link voltage for HOSM and backstepping control (V) (Case 2)

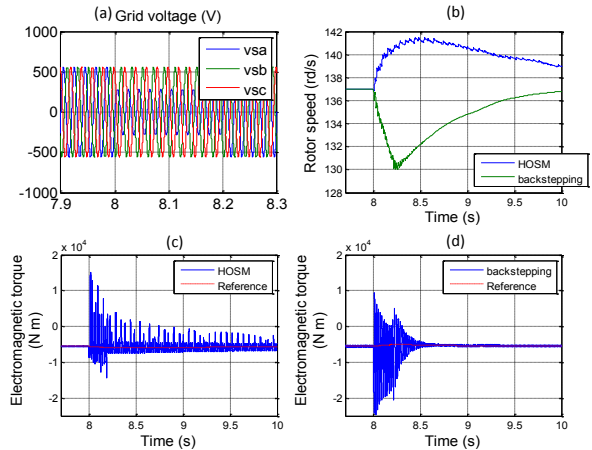


Fig. 12 Results of Case 3; (a) Single-phase voltage dips (50% faults) (V), (b) Rotor speed (rd/s); (c) Electromagnetic torque of HOSM controller (N m); (d) Electromagnetic torque of backstepping controller (N m)

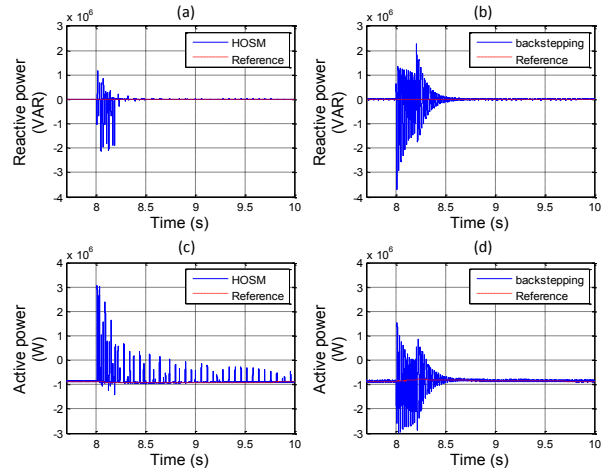


Fig. 13 Results of Case 3; (a) Reactive stator power response of HOSM controller (VAR); (b) Reactive stator power response of backstepping controller (VAR); (c) Active stator power response of HOSM controller (W); (d) Active stator power response of Backstepping controller (W)

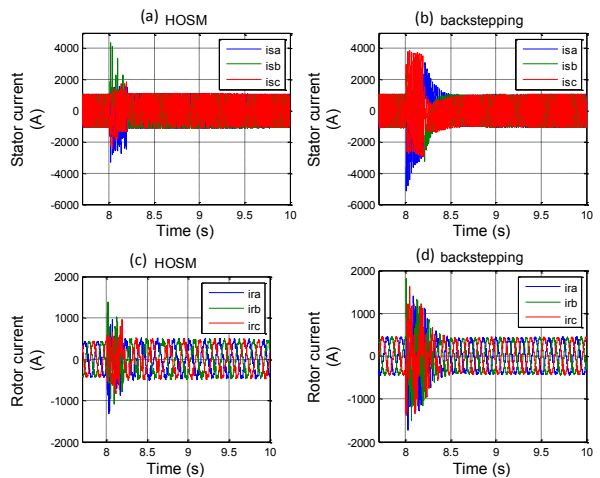


Fig. 14 Results of Case 3; (a) Stator current of HOSM controller (A); (b) Stator current of Backstepping controller; (c) Rotor current of HOSM controller (A); (d) Rotor current of Backstepping controller

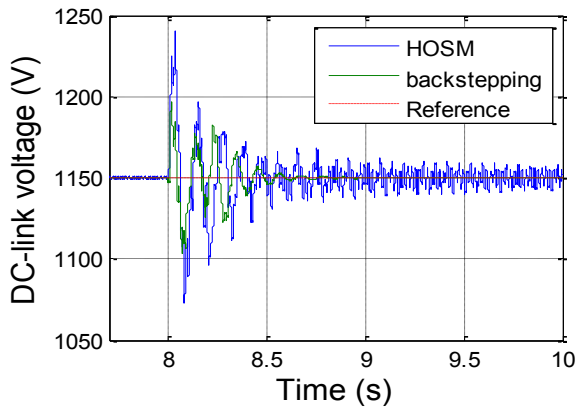


Fig. 15 DC-link voltage for HOSM and backstepping control (V) (Case 3)

fell within acceptable ranges. Notably, when comparing the backstepping technique to the HOSM technique in this specific scenario, it became evident that the former exhibited a lower overshoot in the DC-link voltage response.

Case 3: Single-phase faults: Figs. 12–15 present the system response to a 50% grid voltage dip of phase "a" between 8 s and 8.2 s for the controllers (HOSM control and backstepping control). The HOSM controller still guarantees better performance than backstepping in term of overshooting and time recovery.

Case 4: Frequency variation: wind power generators have to be dimensioned to generate continuous power within the typical grid frequency variations range [24].

The two control methods are tested regarding a frequency variation. The frequency falls from 50 Hz to 47.5 Hz from 8 s to 8.15 s [16].

Figs. 16–19 show the system response to frequency faults of grid voltage between 8 s and 8.2 s for the controllers (HOSM control and backstepping control).

Both controllers did not show satisfactory results. The responses to the tracking references of electromagnetic torque, stator active and reactive power have big overshooting. In terms of time recovery, the backstepping controller recovers more rapidly than HOSM. Moreover, the current ranges are deemed unacceptable.

5 Conclusion

Stator active and reactive powers of DFIG-WT are directly controlled by two robust controllers.

These two controllers are studied under grid fault conditions. The first control technique is HOSM based on the Super twisting algorithm, and the second is the backstepping method. We have provided 4 cases to compare the performances of the controllers. Both control methods show favourable results in the case of a low voltage grid. Furthermore,

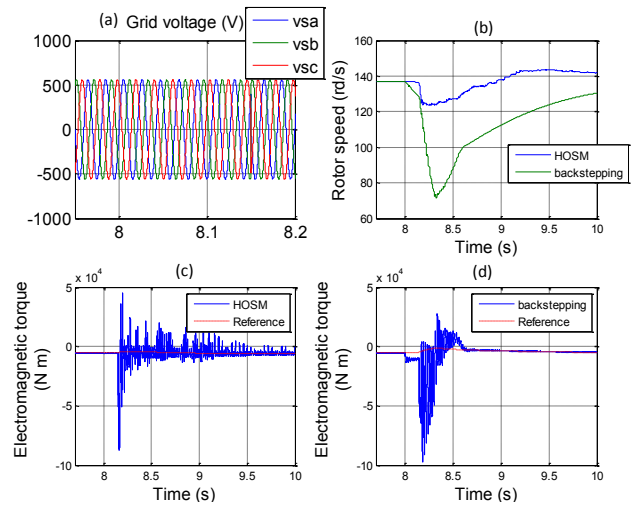


Fig. 16 Results of Case 4; (a) Grid voltage with frequency variation (47.5 Hz from 8–8.15 s) (V); (b) Rotor speed (rd/s); (c) Electromagnetic torque of HOSM controller (N m), (d) Electromagnetic torque of backstepping controller (N m)

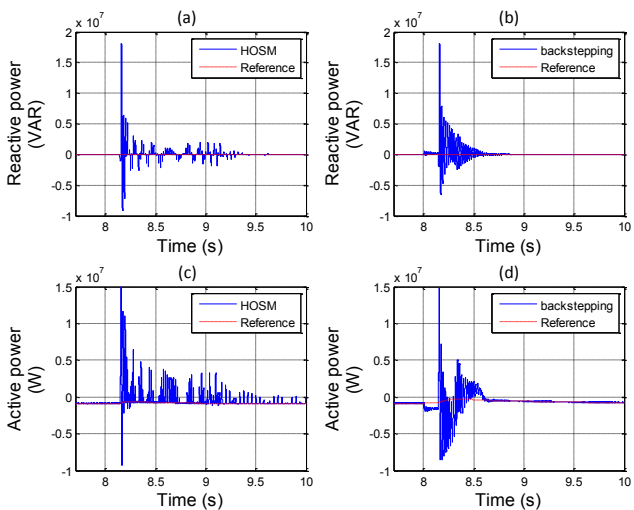


Fig. 17 Results of Case 4; (a) Reactive stator power response of HOSM controller (VAR); (b) Reactive stator power response of Backstepping controller (VAR); (c) Active stator power response of HOSM controller (W); (d) Active stator power response of Backstepping controller (W)

the controllers' effectiveness is more sensitive to the unbalanced voltage faults. However, we notice that the HOSM have better performance in the senses of time recovery and overshooting. In addition, the HOSM is simple to implement and do not need system parameter values. The only inconvenience is the chattering phenomenon, which affects the robustness of the controller after the recovery time.

The performance of controllers under the unbalanced fault grid can be enhanced by introducing the controller to sequence decomposition.

For the security of the converter, we recommend adding a crowbar in the event of a frequency variation grid.

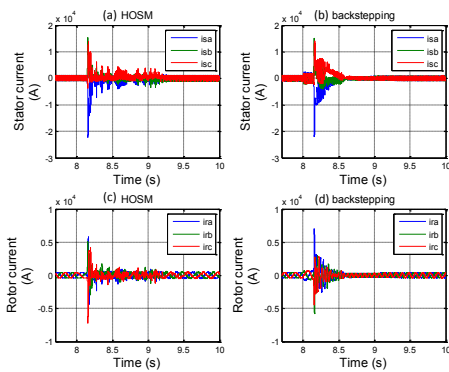


Fig. 18 Results of Case 4; (a) Stator current of HOSM controller (A); (b) Stator current of Backstepping controller, (c) Rotor current of HOSM controller (A), (d) Rotor current of Backstepping controller

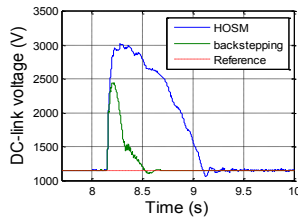


Fig. 19 DC-link voltage for HOSM and backstepping control (V) (Case 4)

References

[1] Roberts, C. "Review of International Grid Codes", Lawrence Berkeley National Laboratory, U.S. Department of Energy, Berkeley, CA, USA, LBNL-2001104, 2018. [online] Available at: <https://escholarship.org/uc/item/5sv540qx> [Accessed: 11 October 2022]

[2] Wu, Y.-K., Chang, S.-M., Mandal, P. "Grid-connected wind power plants: A survey on the integration requirements in modern grid codes", In: 2019 IEEE/IAS 55th Industrial and Commercial Power Systems Technical Conference (I&CPS), Calgary, AB, Canada, 2019, pp. 1–9. ISBN 978-1-5386-7552-6 <https://doi.org/10.1109/icps.2019.8733382>

[3] Mohseni, M., Islam, S. M. "Review of international grid codes for wind power integration: Diversity, technology and a case for global standard", Renewable and Sustainable Energy Reviews, 16(6), pp. 3876–3890, 2012. <https://doi.org/10.1016/j.rser.2012.03.039>

[4] Abdoune, K., Abdoune, F., Aouzellag, D., Ghedamsi, K. "Improved Voltage Harmonics Compensation Strategy for a Stand-Alone DFIG Operating under Unbalanced and Nonlinear Load Conditions", Periodica Polytechnica Electrical Engineering and Computer Science, 64(2), pp. 144–156, 2020. <https://doi.org/10.3311/ppce.15029>

[5] Abad, G., López, J., Rodríguez, M. A., Marroyo, L., Iwanski, G. "Doubly Fed Induction Machine: Modeling and Control for Wind Energy Generation", Institute of Electrical and Electronics Engineers, Inc., 2011. ISBN 9780470768655 <https://doi.org/10.1002/9781118104965>

[6] Ghefiri, K., Bouallègue, S., Garrido, I., Garrido, A. J., Haggège, J. "Complementary Power Control for Doubly Fed Induction Generator-Based Tidal Stream Turbine Generation Plants", Energies, 10(7), 862, 2017. <https://doi.org/10.3390/en10070862>

Nomenclature

w_s, w_r	synchronous and rotor angular frequencies (rad/s)
g	slip (%)
L_s, L_r, L_m	stator, rotor and mutual inductances (H)
R_s, R_r	stator and rotor resistances (Ω)
σ	leakage coefficient
$v_{sd}, v_{sq}, v_{rd}, v_{rq}$	stator and rotor d - q frame voltages (V)
$i_{sd}, i_{sq}, i_{rd}, i_{rq}$	stator and rotor d - q frame currents (A)
$\varphi_{sd}, \varphi_{sq}, \varphi_{rd}, \varphi_{rq}$	stator and rotor d - q frame fluxes (A)
P_s	stator active power (W)
Q_s	stator reactive power (VAR)
u	stator/rotor turns ratio

[7] Karad, S., Thakur, R. "Recent Trends of Control Strategies for Doubly Fed Induction Generator Based Wind Turbine Systems: A Comparative Review", Archives of Computational Methods in Engineering, 28(1), pp. 15–29, 2021. <https://doi.org/10.1007/s11831-019-09367-3>

[8] Morshed, M. J., Fekih, A. "Design of a chattering-free integral terminal sliding mode approach for DFIG-based wind energy systems", Optimal Control Applications and Methods, 41(5), pp. 1718–1734, 2020. <https://doi.org/10.1002/oca.2635>

[9] Abolvafaei, M., Ganjefar, S. "Maximum power extraction from wind energy system using homotopy singular perturbation and fast terminal sliding mode method", Renewable Energy, 148, pp. 611–626, 2020. <https://doi.org/10.1016/j.renene.2019.10.150>

[10] Patnaik, R. K., Dash, P. K. "Fast adaptive finite-time terminal sliding mode power control for the rotor side converter of the DFIG based wind energy conversion system", Sustainable Energy, Grids and Networks, 1, pp. 63–84, 2015. <https://doi.org/10.1016/j.segan.2015.01.002>

[11] Xiong, L., Li, P., Wang, J. "High-order sliding mode control of DFIG under unbalanced grid voltage conditions", International Journal of Electrical Power & Energy Systems, 117, 105608, 2020. <https://doi.org/10.1016/j.ijepes.2019.105608>

[12] Xiong, L., Li, P., Wu, F., Ma, M., Khan, M. W., Wang, J. "A coordinated high-order sliding mode control of DFIG wind turbine for power optimization and grid synchronization", International Journal of Electrical Power & Energy Systems, 105, pp. 679–689, 2019. <https://doi.org/10.1016/j.ijepes.2018.09.008>

- [13] Utkin, V. "Discussion Aspects of High-Order Sliding Mode Control", *IEEE Transactions on Automatic Control*, 61(3), pp. 829–833, 2016.
<https://doi.org/10.1109/tac.2015.2450571>
- [14] Levant, A. "Quasi-continuous high-order sliding-mode controllers", *IEEE Transactions on Automatic Control*, 50(11), pp. 1812–1816, 2005.
<https://doi.org/10.1109/tac.2005.858646>
- [15] Li, Q., Teng, Q., Wang, Y., Ma, X. "Application of High-Order Sliding Mode variable structure Control based on Power-function in Doubly Fed Induction Generator", In: 2018 IEEE International Conference of Intelligent Robotic and Control Engineering (IRCE), Lanzhou, China, 2018, pp. 144–148. ISBN 978-1-5386-7417-8
<https://doi.org/10.1109/irce.2018.8492963>
- [16] Benbouzid, M., Beltran, B., Amirat, Y., Yao, G., Han, J., Mangel, H. "High-Order Sliding Mode control for DFIG-based Wind Turbine Fault Ride-Through", In: 2013 - 39th Annual Conference of the IEEE Industrial Electronics Society, Vienna, Austria, 2013, pp. 7670–7674. ISBN 978-1-4799-0224-8
<https://doi.org/10.1109/iecon.2013.6700411>
- [17] Bossoufi, B., Karim, M., Taoussi, M., Aroussi, H. A., Bouderbala, M., Deblecker, O., Motahhir, S., Nayyar, A., Alzain, M. A. "Rooted tree optimization for the backstepping power control of a doubly fed induction generator wind turbine: Dspace implementation", *IEEE Access*, 9, pp. 26512–26522, 2021.
<https://doi.org/10.1109/access.2021.3057123>
- [18] Roy, T. K., Ghosh, S. K., Anower, M. S., Mahmud, M. A., Kumar, R., Saxena, A. "Mitigation of SSR in Series-Compensated DFIG-Based Wind Farms with STATCOMs using a Nonlinear Backstepping Control Scheme", In: 2020 IEEE International Conference on Power Electronics, Drives and Energy Systems (PEDES), Jaipur, India, 2020, pp. 1–6. ISBN 978-1-7281-5673-6
<https://doi.org/10.1109/pedes49360.2020.9379685>
- [19] Égető, T., Farkas, B. "Model Reference Adaptive System for the Online Rotor Resistance Estimation in the Slip-Ring Machine Based Test-bench", *Periodica Polytechnica Electrical Engineering and Computer Science*, 62(4), pp. 149–154, 2018.
<https://doi.org/10.3311/ppee.12495>
- [20] Kerkoul, B., Boumediene, A. "Stability analysis and study between classical sliding mode control (SMC) and super twisting algorithm (STA) for doubly fed induction generator (DFIG) under wind turbine", *Energy*, 214, 118871, 2021.
<https://doi.org/10.1016/j.energy.2020.118871>
- [21] Fang, X., Tian, Z., Li, H., Yang, Z., Lin, F., Hillmansen, S. "Current closed-loop control and field orientation analysis of an induction motor in six-step operation for railway applications", *IET Power Electronics*, 12(6), pp. 1462–1469, 2019.
<https://doi.org/10.1049/iet-pel.2018.5854>
- [22] Kumar, B., Sandhu, K. S., Sharma, R. "Comparative Analysis of Control Schemes for DFIG-Based Wind Energy System", *Journal of The Institution of Engineers (India): Series B*, 103(2), pp. 649–668, 2022.
<https://doi.org/10.1007/s40031-021-00660-z>
- [23] Khadke, P., Patne, N., Bolisetty, S. "Fault classification and faulty phase selection using symmetrical components of reactive power for EHV transmission line", In: Malik, H., Srivastava, S., Sood, Y., Ahmad, A. (eds) *Applications of Artificial Intelligence Techniques in Engineering. Advances in Intelligent Systems and Computing*, Springer, 2019, pp. 31–42. ISBN 978-981-13-1818-4
https://doi.org/10.1007/978-981-13-1819-1_4
- [24] Morshed, M. J., Fekih, A. "A fault-tolerant control paradigm for microgrid-connected wind energy systems", *IEEE Systems Journal*, 12(1), pp. 360–372, 2018.
<https://doi.org/10.1109/jsyst.2016.2531718>

Appendix

DFIG parameters of 2MW wind turbine:

$$L_s = 0.0026 \text{ H}, L_r = 0.0026 \text{ H}, L_m = 0.0025 \text{ H}, \\ R_s = 0.0026 \Omega, R_r = 0.0029 \Omega.$$

Other parameters are as follows:

$$v_s = 690 \text{ V}, f = 50 \text{ Hz}, w_s = 2 \pi f, u = 1/3.$$